Acta Crystallographica Section F
Structural Biology and Crystallization Communications
ISSN 1744-3091

Structure of the endonuclease IV homologue from *Thermotoga maritima* in the presence of active-site divalent metal ions

Stephen J. Tomanicek,[a]‡ Ronny C. Hughes,[a,b]‡ Joseph D. Ng[b] and Leighton Coates[a]*

[a]Oak Ridge National Laboratory, Neutron Scattering Science Division, 1 Bethel Valley Road, Oak Ridge, TN 37831, USA, and [b]Laboratory for Structural Biology, Department of Biological Sciences, University of Alabama in Huntsville, Huntsville, AL 35899, USA

‡ These authors contributed equally to this work.

Correspondence e-mail: coatesl@ornl.gov

Received 27 April 2010
Accepted 16 July 2010

PDB References: *T. maritima* endonuclease IV, 2x7v; 2x7w.

The most frequent lesion in DNA is at apurinic/apyrimidinic (AP) sites resulting from DNA-base losses. These AP-site lesions can stall DNA replication and lead to genome instability if left unrepaired. The AP endonucleases are an important class of enzymes that are involved in the repair of AP-site intermediates during damage-general DNA base-excision repair pathways. These enzymes hydrolytically cleave the 5′-phosphodiester bond at an AP site to generate a free 3′-hydroxyl group and a 5′-terminal sugar phosphate using their AP nuclease activity. Specifically, *Thermotoga maritima* endonuclease IV is a member of the second conserved AP endonuclease family that includes *Escherichia coli* endonuclease IV, which is the archetype of the AP endonuclease superfamily. In order to more fully characterize the AP endonuclease family of enzymes, two X-ray crystal structures of the *T. maritima* endonuclease IV homologue were determined in the presence of divalent metal ions bound in the active-site region. These structures of the *T. maritima* endonuclease IV homologue further revealed the use of the TIM-barrel fold and the trinuclear metal binding site as important highly conserved structural elements that are involved in DNA-binding and AP-site repair processes in the AP endonuclease superfamily.

1. Introduction

DNA replication and repair processes are essential for maintaining the fidelity and genomic stability required for life. Abasic or apurinic/apyrimidinic (AP) sites are the most common DNA lesions that occur as a result of DNA-base losses. AP sites are generated by the action of damage-specific DNA glycosylases that remove mismatched and modified bases from the damaged DNA (Krokan *et al.*, 1997; Cunningham, 1997; Mol *et al.*, 2000). AP sites can also be generated by direct interactions between DNA and reactive oxygen species, spontaneous hydrolysis, chemical toxins and radiation (Hutchinson, 1985; Lindahl *et al.*, 1997; Huffman *et al.*, 2005). These AP-site lesions can stall DNA replication and if left unrepaired can be mutagenic, leading to genome instability (Loeb & Preston, 1986; Sobol *et al.*, 2003). The repair of AP-site intermediates is initiated by a class of enzymes that are referred to as AP endonucleases (Doetsch & Cunningham, 1990). During damage-general DNA base-excision repair (BER), these enzymes hydrolytically cleave the 5′-phosphodiester bond at an AP site to generate a free 3′-hydroxyl group and a 5′-terminal sugar phosphate (Bailly & Verly, 1989; Levin & Demple, 1990). Following cleavage of the DNA backbone, a DNA deoxyribophosphodiesterase enzyme removes the terminal 5′ sugar phosphate, resulting in a single-nucleotide gap that can be processed by a DNA polymerase and a DNA ligase to complete the repair process (Barzilay & Hickson, 1995; Levin *et al.*, 1988).

The AP endonuclease superfamily is comprised of two conserved families of enzymes that catalyze the first damage-general step of BER by cleaving the DNA backbone immediately 5′ to an AP-site (Aravind *et al.*, 1999). The first enzyme family is typified by exonuclease III (ExoIII; Doetsch & Cunningham, 1990) from *Escherichia coli* and the homologous APE-1 (also known as APEX1; Demple *et al.*, 1991) enzyme in humans. The second conserved AP

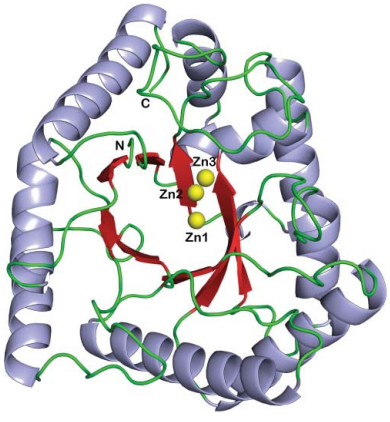

endonuclease family is typified by the functionally related but structurally distinct endonuclease IV (EndoIV; Ramotar, 1997; Hosfield *et al.*, 1999) from *E. coli*, which is considered to be the archetype for the AP endonuclease superfamily. The thermally stable endonuclease IV homologue from the thermophilic bacterium *Thermotoga maritima* (Haas *et al.*, 1999; Hughes *et al.*, 2009) described here is a member of the second conserved AP endonuclease family. Based on functional homology within the AP endonuclease superfamily, the first damage-general step of BER in which AP-site intermediates are processed is highly conserved from bacteria to humans and archaea (Mol *et al.*, 2000; Huffman *et al.*, 2005; Hitomi *et al.*, 2007). Thus, the endonuclease IV enzymes play a major role in cellular DNA-repair pathways by processing AP-site intermediates.

In addition to AP endonuclease activity, the endonuclease IV enzymes also possess additional 3′-processing activities (Demple *et al.*, 1986), act as 3′-to-5′ exonucleases on nicked substrates (Kerins *et al.*, 2003; Ishchenko *et al.*, 2005) and catalyze nucleotide-incision repair (Ischenko & Saparbaev, 2002; Ishchenko *et al.*, 2003), bypassing base removal by glycosylases. Specifically, the *T. maritima* endonuclease IV homologue has been shown to have AP endonuclease activity and also possesses both phosphomonoesterase and phosphodiesterase repair activities on 3′ DNA-blocking groups such as 3′-phosphates, 3′-phosphoglycolates and 3′-*trans*-4-hydroxy-2-pentenal-5-phosphates (Haas *et al.*, 1999) at DNA-strand breaks that result from oxidative DNA damage (Demple *et al.*, 1986). The *T. maritima* endonuclease IV exhibits enzymatic activity at both low and high temperatures and is more thermally stable than the *E. coli* endonuclease IV, with denaturation temperatures approaching 363 K for the *T. maritima* enzyme (Haas *et al.*, 1999).

Previous structural studies of the *E. coli* endonuclease IV enzyme have revealed the use of the widely occurring TIM-barrel fold for recognition and cleavage of DNA at AP sites. In particular, ultrahigh-resolution structures of the DNA-free *E. coli* endonuclease IV [PDB codes 1qtw (Hosfield *et al.*, 1999) and 2nqh (Garcin *et al.*, 2008)] have shown that the active-site region contains three bound zinc ions that are ligated by conserved amino-acid residues. Structures of *E. coli* endonuclease IV complexed with AP-DNA substrate (PDB code 2nqj; Garcin *et al.*, 2008) and AP-DNA product [PDB codes 1qum (Hosfield *et al.*, 1999) and 2nq9 (Garcin *et al.*, 2008)] have revealed the active-site geometry in the presence of trinuclear zinc before and after catalysis. These structures further characterized the DNA-binding specificity of the endonuclease IV family of enzymes, leading to a more complete understanding of the catalytic mechanism (Mol *et al.*, 2000; Hosfield *et al.*, 1999; Garcin *et al.*, 2008).

As a result of efforts to clone, overexpress and crystallize multiple endonuclease IV gene-product homologues, we obtained crystals of the endonuclease IV homologue from *T. maritima* that were suitable for X-ray diffraction experiments (Hughes *et al.*, 2009). Here, we report two X-ray crystal structures of the *T. maritima* endonuclease IV homologue in the presence of divalent metal ions bound in the active-site region. Our interest in determining these structures of *T. maritima* endonuclease IV bound to divalent metal ions was to obtain X-ray structural models for future neutron diffraction studies of the enzyme once larger crystal volumes could be obtained. One structure of the *T. maritima* endonuclease IV, which was solved to 2.30 Å resolution, contained three zinc ions bound in the active-site region. The second structure, which was solved to 2.36 Å resolution, contained a possible mixed-metal configuration of two cadmium ions and one zinc ion bound in the active-site region. These structures of the *T. maritima* endonuclease IV enzyme have further established the binding of trinuclear metal ions as a necessary motif for the AP endonuclease family of enzymes. A structural analysis of the *T. maritima* endonuclease IV active-site regions in the presence of the respective divalent metal ions is presented here.

2. Materials and methods

2.1. Protein expression and purification

A synthetic gene encoding the full-length endonuclease IV homologue (287 amino acids) from *T. maritima* (Q9WYJ7) was designed with *E. coli* codon preference by iXpressGenes Inc. and inserted into a pET3a expression plasmid (Novagen) by recombining the *Bam*HI- and *Nde*I-restricted linear expression vector and the PCR product using *in vivo* homologous recombination in DH5α competent *E. coli* as described by Marsic *et al.* (2008). Recombinant endonuclease IV from *T. maritima* was expressed in *E. coli* and purified as described previously by Hughes *et al.* (2009). SDS–PAGE was used to confirm the homogeneity of the purified protein. The purified protein was then concentrated by centrifugation (Millipore Amicon Ultra, 10 000 molecular-weight cutoff) and the protein concentration was determined by UV absorbance ($A_{280\,\mathrm{nm}}$ = 0.95 for 1 mg ml^{-1}). Prior to crystallization, all concentrated protein samples were filtered using 0.45 µm Ultra-free MC spin filters (Millipore, USA).

2.2. Crystallization

Following purification, the enzyme was prepared in a buffer solution consisting of 0.05 *M* MOPS pH 8.0 and 0.05 *M* NaCl and the protein solution was concentrated to 10 mg ml^{-1} for crystallization. Crystals of endonuclease IV from *T. maritima* with cadmium and zinc were obtained using the sitting-drop vapor-diffusion method at 295 K in a 96-well Intelli-Plate (Art Robbins) as previously described by Hughes *et al.* (2009). In the setup, the sitting-drop well contained 3 µl protein solution mixed with 3 µl reservoir solution [0.1 *M* Bicine pH 9.0, 20%(*w*/*v*) polyethylene glycol MME 550] and 1 µl of a microcrystalline seeding stock. The volume of the reservoir solution was 100 µl. The seeding stock used for crystallization was the well solution from Crystal Screen HT (Hampton Research) condition G10 (0.05 *M* cadmium sulfate hydrate, 0.1 *M* HEPES pH 7.5, 1.0 *M* sodium acetate trihydrate). After one week, well formed rod-shaped crystals were observed (Hughes *et al.*, 2009). While zinc was not intentionally included during crystallization, we hypothesize that unknown trace amounts of divalent zinc throughout sample preparation may account for the presence of zinc in the crystal structure of the mixed-metal configuration (see §3). Prior to data collection, the crystals of endonuclease IV from *T. maritima* with cadmium and zinc were placed momentarily in a reservoir solution containing a cryoprotectant (30% glycerol) and flash-frozen in liquid nitrogen. Crystals of endonuclease IV from *T. maritima* with zinc were obtained as described above followed by soaking the crystals for 10 min in a reservoir solution containing 10 m*M* zinc sulfate and 30% glycerol prior to flash-freezing in liquid nitrogen for data collection.

2.3. X-ray diffraction data collection and processing

For data collection, single crystals of endonuclease IV from *T. maritima* in the presence of the respective divalent metal ions were placed momentarily in a reservoir solution containing cryoprotectant (30% glycerol) and flash-frozen in liquid nitrogen. Diffraction data for *T. maritima* endonuclease IV with zinc were collected over a range of 70° (1° steps) using a MAR Research MX-300 detector on the SER-CAT 22-BM beamline (λ = 1.00 Å) at the Advanced Photon Source (Chicago, USA). The data were processed to 2.30 Å resolu-

Table 1
Data-collection and refinement statistics.

Values in parentheses are for the highest resolution shell.

	With Zn (PDB code 2x7v)	With Cd and Zn (PDB code 2x7w)
Unit-cell parameters (Å)	$a = b = 123.37$, $c = 35.30$	$a = b = 123.19$, $c = 35.34$
Space group	$P6_1$	$P6_1$
No. of unique reflections	13865	12749
Resolution range (Å)	35.61–2.30 (2.42–2.30)	40.32–2.36 (2.44–2.36)
Multiplicity	4.2 (4.1)	4.3 (4.1)
$I/\sigma(I)$	4.5 (2.1)	13.1 (6.2)
$R_{\rm merge}$† (%)	12.3 (36.0)	9.5 (17.4)
Data completeness (%)	99.4 (99.9)	99.3 (95.6)
R factor‡ (%)	14.6	15.6
$R_{\rm free}$‡ (%)	20.0	19.6
R.m.s.d. bonds§ (Å)	0.009	0.023
R.m.s.d. angles§ (°)	1.103	0.794
Atoms (non-H)	2446	2501
Solvent molecules	165	209
Ramachandran plot¶		
Outliers (%)	0.0	0.0
Favored (%)	98.2	98.6
Rotamer outliers (%)	3.3	1.6

† $R_{\rm merge} = 100 \times \sum_{hkl} \sum_i |I_i(hkl) - \langle I(hkl)\rangle| \sum_{hkl} \sum_i I_i(hkl)$, where $I_i(hkl)$ is the intensity of reflection hkl and $\langle I(hkl)\rangle$ is the mean value of i multiple measurements of reflection hkl. ‡ R factor $= \sum_{hkl} ||F_{\rm obs}| - |F_{\rm calc}|| / \sum_{hkl} |F_{\rm obs}|$; $R_{\rm free}$ is the R factor computed using a 5% subset of the data randomly excluded from structure determination (where $F_{\rm calc}$ includes all scale factors and corrections for bulk solvent). § Root-mean-square deviations of bond lengths in angstroms and bond angles in degrees calculated with *phenix.refine* in the *PHENIX* program suite. ¶ Ramachandran plot quality assessment using *MolProbity*.

tion using *MOSFLM* (Leslie, 1992); *SCALA* (Collaborative Computational Project, Number 4, 1994) was used to scale and merge the observed data. The crystal of *T. maritima* endonuclease IV with zinc belonged to the hexagonal space group $P6_1$, with unit-cell parameters $a = 123.37$, $b = 123.37$, $c = 35.30$ Å. Diffraction data for *T. maritima* endonuclease IV with cadmium and zinc were collected over a range of 70° (1° steps) using a MAR Research MX-300 detector on the SER-CAT 22-BM beamline (λ = 1.00 Å) at the Advanced Photon Source (Chicago, USA). The data were processed to 2.36 Å resolution using *HKL*-2000; *SCALEPACK* (Otwinowski & Minor, 1997) was used to scale and merge the observed data. The crystal of *T. maritima* endonuclease IV with cadmium belonged to the hexagonal space group $P6_1$, with unit-cell parameters $a = 123.19$, $b = 123.19$, $c = 35.34$ Å. See Table 1 for a summary of all X-ray crystallographic data-collection statistics.

2.4. Structure determination and refinement

The structures of *T. maritima* endonuclease IV in the presence of either three zinc ions or the likely mixed-metal configuration of two cadmium ions and one bound zinc ion were both solved by molecular replacement using the *Phaser* (McCoy *et al.*, 2007) program from the *PHENIX* (Adams *et al.*, 2002) program suite with the known structure of *E. coli* endonuclease IV (PDB code 1qtw; Hosfield *et al.*, 1999) as the search model (32% sequence homology to *T. maritima* endonuclease IV) as described by Hughes *et al.* (2009). The molecular-replacement solution for each respective data set was refined using the *phenix.refine* (Afonine *et al.*, 2005) program in *PHENIX* (v.1.6_289). The final model for each structure was obtained after several rounds of maximum-likelihood-based refinement of individual coordinates, atomic displacement parameters (ADP) and occupancies using the *phenix.refine* program and model building into σ_A-weighted $F_o - F_c$ and $2F_o - F_c$ electron-density maps using *Coot* (Emsley & Cowtan, 2004). In each structure, a total of 286 amino-acid residues were included in the final model; only the C-terminal residue 287 was disordered in the electron-density maps and could not be modeled. The final refinement statistics from *phenix.refine* for each structure are summarized in Table 1. *MolProbity* (Chen *et al.*, 2010) was used to analyze the stereochemistry of the final models (see Table 1). Figures of the models were created and rendered with the program *PyMOL* (DeLano, 2008).

3. Results

3.1. Overall structure of *T. maritima* endonuclease IV

Two X-ray crystal structures of the *T. maritima* endonuclease IV homologue with divalent metal ions bound in the active site were

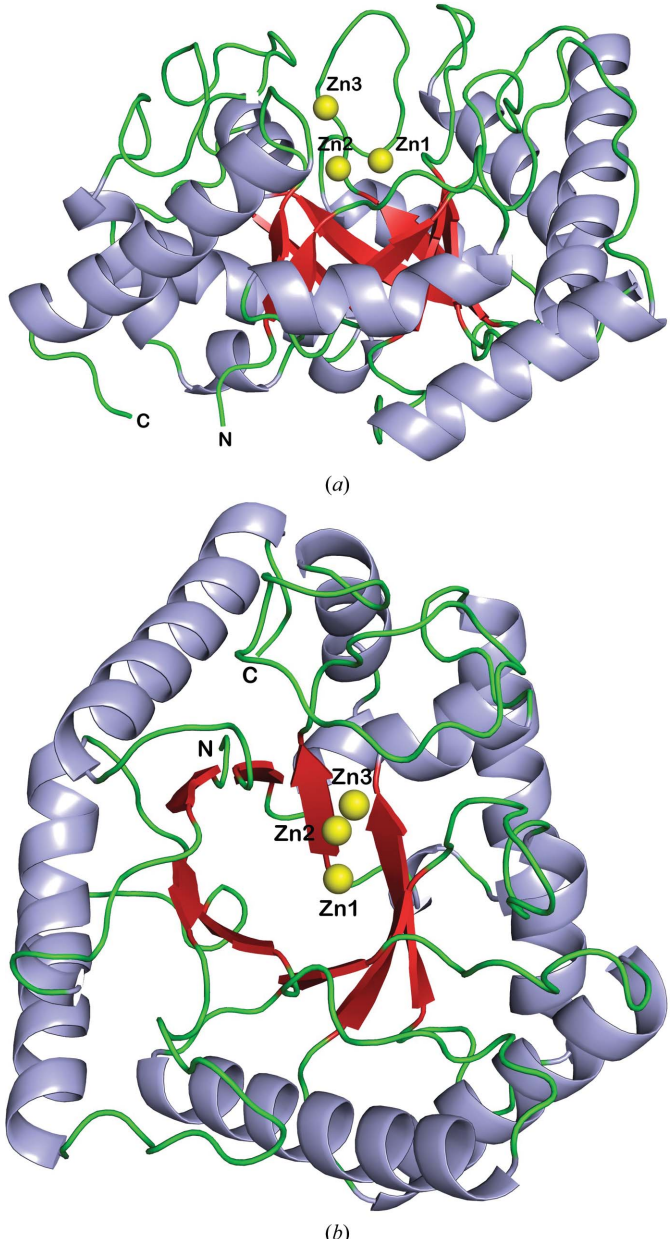

Figure 1
(*a*) Ribbon diagram of *T. maritima* endonuclease IV in the presence of three bound zinc ions (Zn1, Zn2 and Zn3; shown in yellow) as viewed from the side of the $\alpha\beta$-barrel fold, which consists of eight parallel β-strands (shown in red) that are surrounded by eight peripheral α-helices (shown in light blue) and are connected by loop regions (shown in green). (*b*) Ribbon diagram of *T. maritima* endonuclease IV in the presence of three bound zinc ions (Zn1, Zn2 and Zn3) as viewed from the top or the C-terminal face of the $\alpha\beta$-barrel fold (colors are the same as noted in *a*).

determined by molecular replacement. Final models with good stereochemistry were obtained by completing multiple rounds of model building and maximum-likelihood-based individual coordinate, atomic displacement parameter (ADP) and occupancy refinement against X-ray diffraction data (see Table 1). One structure of *T. maritima* endonuclease IV solved to 2.30 Å resolution (R factor = 14.6%; R_{free} = 20.0%) contained three zinc ions bound in the active-site region. The second structure, which was solved to 2.36 Å resolution (R factor = 15.6%; R_{free} = 19.6%), contained a possible mixed-metal configuration of two cadmium ions and one zinc ion bound in the active-site region along with a Bicine buffer molecule. Both structures of *T. maritima* endonuclease IV in the presence of divalent metal ions are essentially identical (r.m.s.d. = 0.12 Å for the main chain), with the only differences being the radii of the respective metal ions and the presence of a Bicine ligand in the structure containing cadmium; therefore, the structure in the presence of three zinc ions is used to describe the overall three-dimensional structure of the enzyme.

T. maritima endonuclease IV is a single-domain $\alpha\beta$ protein in which the secondary-structure elements are arranged as a barrel consisting of eight parallel β-strands that are surrounded by eight peripheral α-helices (see Figs. 1*a* and 1*b*). This eight-stranded $\alpha\beta$-barrel fold was first observed in triose phosphate isomerase (TIM barrel; Banner *et al.*, 1975) and is a major folding superfamily that occurs in a number of enzymes with diverse functions (Farber & Petsko, 1990; Reardon & Farber, 1995). Like other TIM-barrel proteins, all eight peripheral α-helices in the *T. maritima* endonuclease IV structure are oriented with their N-termini pointing towards the C-terminal face of the β-barrel. A large crescent-shaped pocket is formed from five protruding loops that connect the α-helices and β-sheets at the C-terminal face of the β-barrel. These five loops or R-loops have been shown to be involved in the binding of AP-DNA substrate by binding to the phosphate backbone and providing DNA-base interactions at the AP site (Hosfield *et al.*, 1999; Garcin *et al.*, 2008). The base of the large pocket forms the active-site region of the enzyme where three zinc ions are bound to absolutely conserved amino-acid residues (see Figs. 1*a* and 1*b*). Previous structures of *E. coli* endonuclease IV demonstrated how structural features of the TIM-barrel fold, such as the positive helix dipoles pointing toward the C-terminal face of the enzyme and the active-site pocket containing the trinuclear 'mainly' zinc binding site, are optimized for DNA binding (Hosfield *et al.*, 1999; Garcin *et al.*, 2008).

3.2. Metal-ion arrangement in *T. maritima* endonuclease IV

The *T. maritima* endonuclease IV active site, which is located at the base of the pocket formed by the β-barrel, contains three metal ions that are bound to absolutely conserved amino-acid residues. The active-site regions of *T. maritima* endonuclease IV bound to three zinc ions and the likely mixed-metal configuration of two cadmium ions, one zinc ion and a Bicine buffer molecule are shown in Figs. 2(*a*) and 2(*b*), respectively. The locations of all active-site divalent metal ions for each structure were determined based on a thorough analysis of σ_A-weighted $F_o - F_c$ electron-density maps calculated using *phenix.refine* (Afonine *et al.*, 2005). While ambiguous, our interpretation of the electron density for the mixed-metal configuration as containing two cadmium ions and one zinc ion is in agreement with the refined occupancy and B-factor values for these respective metal sites as discussed below. Strong positive electron-density peaks associated with the positions of divalent zinc ions were observed up to contour levels of 21σ for both Zn1 and Zn3 and of 17σ for Zn2. In the cadmium- and zinc-containing structure strong positive electron-density peaks associated with the positions of divalent metal ions were observed up to contour levels of 15σ for both Cd2 and Cd3 and of 8σ for Zn1. The zinc and cadmium divalent metal ions were introduced into the crystals either through soaking experiments (zinc-containing structure) or through crystallization screening and seeding experiments (cadmium- and zinc-containing structure) as described above in §2. In the structure of *T. maritima* endonuclease IV, the bound zinc ions refined to occupancy values of 82, 72 and 92% for Zn1, Zn2 and Zn3, respectively, with refined B-factor values of 24.6, 30.4 and 30.5 Å^2, respectively. In the structure bound to cadmium and zinc, the cadmium ions refined to occupancy values of 100 and 92% for Cd2 and Cd3, respectively, with refined B-factor values of 10.5 and 10.7 Å^2, respectively, and the Zn1 zinc ion refined to an occupancy value of 44%, with a refined B-factor value of 13.5 Å^2. The Bicine buffer molecule bound adjacent to the Cd3 metal site refined to an occupancy value of 97%. As the crystals used for determining the

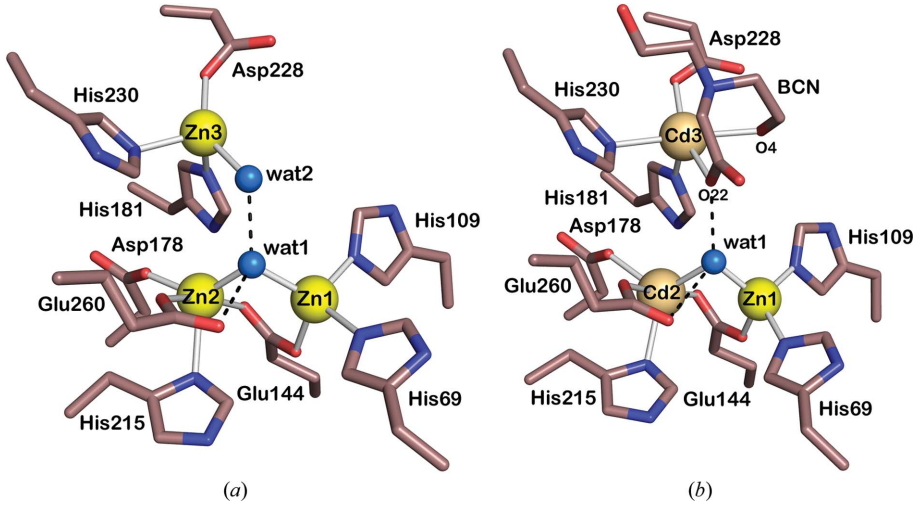

Figure 2
(*a*) Active-site region of *T. maritima* endonuclease IV in the presence of three bound zinc ions (Zn1, Zn2 and Zn3) and two water molecules (wat1 and wat2). Hydrogen-bonding interactions are shown by dashed lines. (*b*) Active-site region of *T. maritima* endonuclease IV in the presence of two bound cadmium ions (Cd2 and Cd3), one bound zinc ion (Zn1) and two water molecules (wat1 and wat2). The active-site region also contains a Bicine buffer molecule (BCN) that is bound adjacent to Cd3. Hydrogen-bonding interactions are shown as dashed lines.

Table 2
Bond distances for the trinuclear metal sites in the active sites of *T. maritima* endonuclease IV and *E. coli* endonuclease IV (PDB code 1qtw; Hosfield *et al.*, 1999).

All bond distances are in Å.

(*a*) *T. maritima* endonuclease IV.

	Structure with Zn	Structure with Cd and Zn
Metal site 1		
Zn1—His109 $N^{\varepsilon 2}$	2.19	2.05
Zn1—His69 $N^{\varepsilon 2}$	2.26	2.08
Zn1—Glu144 $O^{\varepsilon 1}$	2.23	2.08
Zn1—wat1	2.26	2.05
Zn1 geometry	Tetrahedral	Tetrahedral
Metal site 2		
Zn2/Cd2—Glu144 $O^{\varepsilon 2}$	2.26	2.11
Zn2/Cd2—Glu260 $O^{\varepsilon 1}$	2.18	2.28
Zn2/Cd2—His215 $N^{\delta 1}$	2.37	2.36
Zn2/Cd2—Asp178 $O^{\delta 1}$	2.09	2.44
Zn2/Cd2—wat1	2.22	2.45
Zn2/Cd2 geometry	Trigonal bipyramidal	Trigonal bipyramidal
Metal site 3		
Zn3/Cd3—Asp228 $O^{\delta 2}$	2.38	2.33
Zn3/Cd3—His230 $N^{\varepsilon 2}$	2.21	2.51
Zn3/Cd3—His181 $N^{\varepsilon 2}$	2.16	2.31
Zn3—wat2	2.41	—
Cd3—Bicine O22	—	2.42
Cd3—Bicine O4	—	2.54
Zn3/Cd3 geometry	Distorted tetrahedral	Distorted trigonal bipyramidal

(*b*) *E. coli* endonuclease IV.

	Structure with Zn (PDB code 1qtw; Hosfield *et al.*, 1999)
Metal site 1	
Zn1—His109 $N^{\varepsilon 2}$	1.98
Zn1—His69 $N^{\varepsilon 2}$	2.01
Zn1—Glu145 $O^{\varepsilon 2}$	2.07
Zn1—wat1	1.92
Zn1 geometry	Tetrahedral
Metal site 2	
Zn2—Glu145 $O^{\varepsilon 1}$	2.11
Zn2—Glu261 $O^{\varepsilon 1}$	2.21
Zn2—His216 $N^{\delta 1}$	2.07
Zn2—Asp179 $O^{\delta 2}$	1.98
Zn2—wat1	2.00
Zn2 geometry	Trigonal bipyramidal
Metal site 3	
Zn3—Asp229 $O^{\delta 1}$	2.19
Zn3—Asp229 $O^{\delta 2}$	2.34
Zn3—His231 $N^{\varepsilon 2}$	1.98
Zn3—His182 $N^{\varepsilon 2}$	2.00
Zn3—wat2	2.01
Zn3—wat3	2.39
Zn3 geometry	Distorted trigonal bipyramidal

cadmium and zinc structure were grown by seeding techniques in the presence of cadmium as previously described in our crystallization report (Hughes *et al.*, 2009), the metal ion bound in site 1 could also be a partially occupied cadmium ion. The refined occupancy value for a cadmium ion (Cd1) bound in metal site 1 was 35% (data not shown). Additional refinements were also completed with zinc ions in both metal sites 2 and 3 in order to confirm the presence of the heavier cadmium ions. An analysis of σ_A-weighted $F_o - F_c$ electron-density maps along with refined ADP and occupancy values confirmed that metal sites 2 and 3 are most likely to be occupied by cadmium ions (data not shown). In particular, when a zinc ion was refined in metal site 2 additional $F_o - F_c$ electron density was present around the position of the refined zinc, providing further evidence that metal site 2 is likely to be occupied by the heavier cadmium ion (data not shown). While zinc was not intentionally included in the cell-culture media, purification buffers or crystallization screening reagents, the presence of unknown trace amounts of divalent zinc throughout sample preparation may account for the presence of a partially bound zinc ion in metal site 1.

In the structure of *T. maritima* endonuclease IV bound to three zinc ions, both Zn1 and Zn2 are located at the base of the pocket formed by the β-barrel and are separated by 3.37 Å. The third bound zinc ion, Zn3, is displaced away from the base of the pocket and from both Zn1 and Zn2, with a Zn1–Zn3 distance of 5.94 Å and a Zn2–Zn3 distance of 4.85 Å (see Fig. 2*a*). Based on its location in the active-site pocket, Zn3 is more solvent-accessible than both Zn1 and Zn2. The Zn1 ion is coordinated by the side chains of His69, His109, Glu144 and water molecule 1 (wat1) in a tetrahedral arrangement. Both the side chain of Glu144 and wat1 bridge between the bound Zn1 and Zn2 ions. It has been hypothesized that the bridging water molecule (wat1) is likely to be the nucleophile in the phosphodiester-hydrolysis reaction once it has been deprotonated (Garcin *et al.*, 2008; Ivanov *et al.*, 2007). The Zn2 ion is coordinated by the side chains of Glu144, Asp178, Glu260, His215 and wat1 in a trigonal bipyramidal arrangement in which Glu144 and Glu260 are axial ligands and Asp178, Glu260 and wat1 are equatorial ligands. The displaced Zn3 ion is coordinated in a distorted tetrahedral arrangement to the side chains of His181, Asp228, His230 and water molecule 2 (wat2) as shown in Fig. 2(*a*). A summary of the bond distances in the active-site region of *T. maritima* endonuclease IV bound to zinc is given in Table 2.

The overall active-site structure of *T. maritima* endonuclease IV bound to cadmium and zinc is quite similar to the structure bound to zinc: both Zn1 and Cd2 are also located at the base of the β-barrel and are separated by 3.25 Å. Similarly, the third bound ion, Cd3, is also displaced away from the base of the pocket and from both Zn1 and Cd2, with a Zn1—Cd3 distance of 5.85 Å and a Cd2—Cd3 distance of 5.14 Å (see Fig. 2*b*). The coordination of amino-acid side chains around metal sites 1 and 2 in the presence of zinc and cadmium, respectively, is identical to that of the zinc-bound structure; Zn1 is coordinated in a tetrahedral arrangement and Cd2 is coordinated in a trigonal bipyramidal arrangement. The coordination of Cd3 in the third metal site is different from the zinc-bound structure owing to the displacement of wat2 by the Bicine buffer molecule. The Cd3 ion is coordinated in a distorted trigonal bipyramidal arrangement to the side chains of His181, Asp228 and His230 and to the anionic Bicine buffer molecule, which forms a bidentate ligand to Cd3 (see Fig. 2*b*) through Bicine O4 and O22. The complexation of divalent transition-metal ions with zwitterionic buffers such as Bicine is well known (Corfu & Bin Song, 1992). A summary of the bond distances in the active-site region of *T. maritima* endonuclease IV bound to two cadmium ions and one zinc ion is given in Table 2.

3.3. Structure comparison of *T. maritima* endonuclease IV and *E. coli* endonuclease IV

Endonuclease IV from *E. coli* is considered to be the archetype for the second conserved AP endonuclease superfamily of enzymes (Ramotar, 1997; Hosfield *et al.*, 1999). It has been shown that *T. maritima* endonuclease IV is a member of the second conserved AP endonuclease family as a result of its possessing enzymatic activities that are characteristic of the endonuclease IV family of DNA-repair enzymes, including AP endonuclease activity and repair activities on 3′-phosphates, 3′-phosphoglycolates and 3′-*trans*-4-hydroxy-2-pentenal-5-phosphates (Haas *et al.*, 1999). Based on a primary sequence alignment, *T. maritima* endonuclease IV has only 32% sequence identity to *E. coli* endonuclease IV (see Fig. 3). A superposition of the ribbon structures of both *T. maritima* endonuclease IV and *E. coli* endonuclease IV (PDB code 1qtw; Hosfield *et*

al., 1999) bound to trinuclear zinc is shown in Fig. 4(*a*). The secondary-structure matching program within *Coot* was used for all structure superpositions (Krissinel & Henrick, 2004). Even with such a low sequence identity, the overall structural folds of these enzymes are remarkably similar, with an r.m.s.d. of 1.65 Å for main-chain atoms. Both enzymes have the characteristic TIM-barrel fold (Marsic *et al.*, 2008) consisting of eight parallel β-strands that are surrounded by eight peripheral α-helices. The active-site pocket formed from the central β-barrel that contains the trinuclear zinc site in each enzyme is also structurally conserved in both *T. maritima* endonuclease IV and *E. coli* endonuclease IV.

Structural differences between these enzymes are present within the five protruding loops (R-loops) that connect the α-helices and β-sheets at the C-terminal face of the β-barrel. The orientations of these loop regions in *T. maritima* endonuclease IV are shifted slightly with respect to their positions in *E. coli* endonuclease IV, with the largest shift (approximately 5 Å) being present in R-loop 2. Smaller main-chain R-loop conformational differences are present between the two enzymes in R-loop 3 (1.05 Å shift), R-loop 4 (1.33 Å shift) and R-loop 4 (1.36 Å shift). It is likely that primary sequence differences within these R-loop regions (see Fig. 3) and crystal lattice contacts involving these R-loop regions account for these structural differences between *T. maritima* endonuclease IV and *E. coli* endonuclease IV. In *E. coli* endonuclease IV, conformational changes in these loop regions have been shown to be important for binding AP-DNA substrate. Specifically, residues Arg37 (R-loop 2) and Tyr72

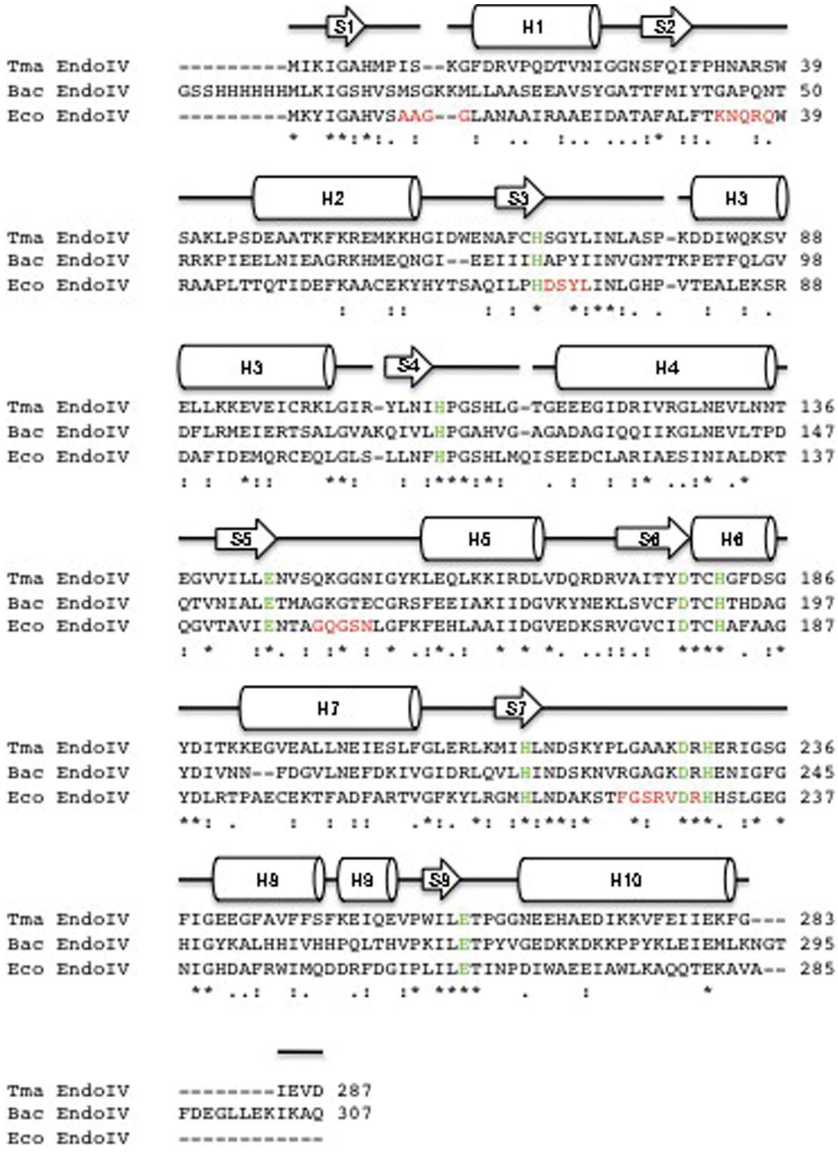

Figure 3
Amino-acid sequence alignment of *T. maritima* endonuclease IV (287 residues), *E. coli* endonuclease IV (285 residues) and *Bacillus anthracis* endonuclease IV (307 residues). The amino-acid sequences of *T. maritima* endonuclease IV (Tma EndoIV; Q9WYJ7), *E. coli* endonuclease IV (Eco EndoIV; P0A6C1) and *B. anthracis* endonuclease IV (Bac EndoIV; Q81LV1) from PDB code 1xp3 (M. J. Fogg, V. M. Levdikov, E. V. Blagova, J. A. Brannigan, A. J. Wilkinson & K. S. Wilson, unpublished work) were aligned with the program *ClustalW* (Thompson *et al.*, 1994). The secondary-structure elements of *T. maritima* endonuclease IV bound to zinc are shown aligned with its primary sequence, where H and S represent α-helices and β-sheets, respectively. The absolutely conserved amino-acid residues in the active-site regions of Tma EndoIV, Eco EndoIV and Bac EndoIV that are involved in the binding of divalent metal ions are colored green. The five R-loop regions (residues 10–13, 34–38, 70–73, 149–153 and 224–230) in *E. coli* endonuclease IV that have been shown to be involved in DNA binding are colored in red below the corresponding residues in both *T. maritima* endonuclease IV and *B. anthracis* endonuclease IV. The '*' symbol indicates identical residues in the sequence alignment, the ':' symbol indicates conserved substitutions in the sequence alignment and the '.' symbol indicates semi-conserved substitutions in the sequence alignment.

(R-loop 3) in *E. coli* endonuclease IV are involved in important minor-groove-penetrating interactions with AP-DNA substrate that result from conformational changes in these respective R-loops (Hosfield *et al.*, 1999; Garcin *et al.*, 2008). In the *T. maritima* endonuclease IV structure, the conserved Arg37 and Tyr72 residues are also located within R-loop 2 and R-loop 3, respectively. In the *T. maritima* endonuclease IV structure the Arg37 side chain is rotated by approximately 30° and is located 4.7 Å away from the center of the β-barrel with respect to the location of Arg37 in *E. coli* endonuclease IV. The position of Tyr72 in the *T. maritima* endonuclease IV structure is in a similar location to that of Tyr72 in *E. coli* endonuclease IV. A comparison of the conformations of residues Arg37 (R-loop 2) and Tyr72 (R-loop 3) in both the *T. maritima* endonuclease IV and *E. coli* endonuclease IV structures is shown in Fig. 4(*b*). In addition to the differences in the R-loop regions, structural differences between the two enzymes are also present in the α-helical regions in their C-terminal regions. The C-terminal α-helical regions (residues 241–249 and 267–282) of *T. maritima* endonuclease IV are shifted outward and away from the central β-barrel region by approximately 2–5 Å in comparison to the positions of these C-terminal regions in *E. coli* endonuclease IV.

Interestingly, even with such a low sequence identity the residues involved in forming the trinuclear metal binding site are absolutely conserved in both *T. maritima* endonuclease IV and *E. coli* endonuclease IV (see Fig. 3). A highly conserved region (residues 171–189) within the second family of AP endonucleases is also present in *T. maritima* endonuclease IV. Analogous to the structure of *E. coli* endonuclease IV (Hosfield *et al.*, 1999), this conserved region in *T. maritima* endonuclease IV also provides important packing and hydrogen-bonding interactions within the central β-barrel that serve to stabilize the relative positions of Zn2 and Zn3 within the trinuclear metal site. In the *E. coli* endonuclease IV structure, Zn1 and Zn2 are located at the base of the β-barrel and are separated by 3.40 Å. The third metal site, Zn3, is displaced from the first two metal centers, with a Zn1–Zn3 distance of 5.43 Å and a Zn2–Zn3 distance of 4.67 Å. The active-site region of *E. coli* endonuclease IV is shown in Fig. 5. A summary of the bond distances in the active-site region of *E. coli* endonuclease IV (Hosfield *et al.*, 1999) bound to trinuclear zinc is shown in Table 2. The overall active-site structure and coordination arrangement around the Zn1 and Zn2 metal ions are nearly identical in both *E. coli* endonuclease IV and *T. maritima* endonuclease IV.

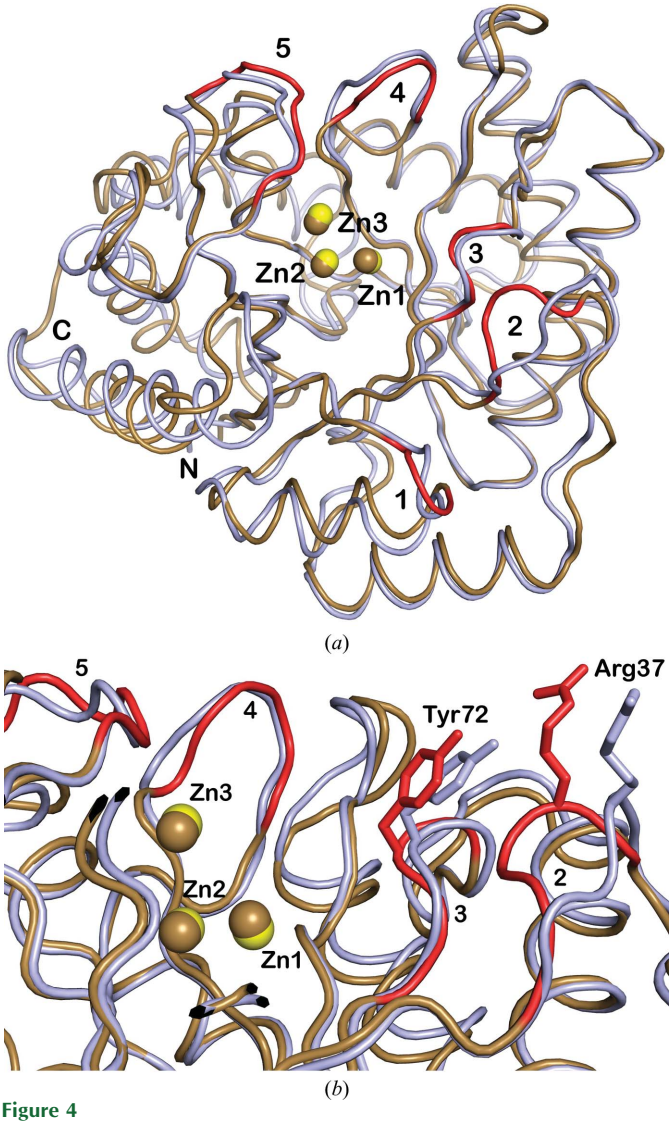

Figure 4
(*a*) Backbone superpostion of the *T. maritima* endonuclease IV and *E. coli* endonuclease IV (PDB code 1qtw; Hosfield *et al.*, 1999) structures both in the presence of three bound zinc ions (Zn1, Zn2 and Zn3). The *T. maritima* endonuclease IV structure is shown in light blue, with the three bound zinc ions colored yellow. The *E. coli* endonuclease IV structure is shown in brown, with the three bound zinc ions also colored brown. The five R-loop regions (residues 10–13, 34–38, 70–73, 149–153 and 224–230) in the *E. coli* endonuclease IV structure are colored red and labeled 1–5, respectively. These five loop regions connect the α-helices and β-sheets at the C-terminal face of the β-barrel and have also been shown to be involved in the binding to AP-DNA substrate (Hosfield *et al.*, 1999; Garcin *et al.*, 2008). Although it only has 32% sequence identity to *E. coli* endonuclease IV, the structure of *T. maritima* endonuclease IV has the same overall $\alpha\beta$-barrel fold consisting of eight parallel β-strands that are surrounded by eight peripheral α-helices. (*b*) Backbone superposition of the *T. maritima* endonuclease IV and *E. coli* endonuclease IV structures, showing a comparison of the conformations of residues Arg37 and Tyr72. The colors of the endonuclease IV enzymes and bound zinc ions are the same as described in (*a*). Four R-loop regions (residues 34–38, 70–73, 149–153 and 224–230) in the *E. coli* endonuclease IV structure are colored red and labeled 2–5, respectively. The positions of Arg37 and Tyr72 in *E. coli* endonuclease IV are colored red, corresponding to their respective locations in R-loop 2 and R-loop 3. The positions of Arg37 and Tyr72 in the *T. maritima* endonuclease IV structure are colored light blue.

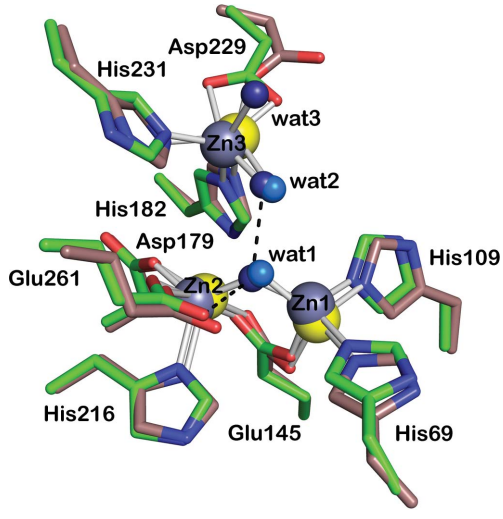

Figure 5
Active-site region of *E. coli* endonuclease IV with C atoms shown in green (PDB code 1qtw; Hosfield *et al.*, 1999) in the presence of three bound zinc ions (Zn1, Zn2 and Zn3, shown in gray) and three water molecules (wat1, wat2 and wat3, shown in dark blue). Hydrogen-bonding interactions are shown by dashed lines. All labels correspond to the *E. coli* endonuclease IV structure. The active-site region of *T. maritima* endonuclease IV from Fig. 2(*a*) in the presence of three bound zinc ions (Zn1, Zn2 and Zn3 shown in yellow) and two water molecules (wat1 and wat2 shown in light blue) is shown superimposed with C atoms in brown.

The only distinct difference within the active-site region between the enzymes is the coordination and arrangement around Zn3. In the *E. coli* endonuclease IV active site the Zn3 ion is coordinated to the side chains of His182, His231 and Asp229 and water molecule 2 (wat2) in a distorted trigonal bipyramidal arrangement. The two side-chain carboxyl O atoms of Asp229 form a unibidentate ligand to Zn3, in contrast to the active site of *T. maritima* endonuclease IV, where only one of the Asp228 carboxyl O atoms can coordinate to Zn3. In the *T. maritima* endonuclease IV structure a conformational change in R-loop 5 (as discussed above and shown in Fig. 4) repositions the side chain of Asp228 so that only one of the carboxyl O atoms can coordinate to Zn3. Also, there is an additional water molecule (wat3) located 2.4 Å away from Zn3 in *E. coli* endonuclease IV that is not present in the *T. maritima* endonuclease IV structure (see Fig. 5). In the structure of the *T. maritima* endonuclease IV structure bound to cadmium and zinc the Cd3 metal ion is also coordinated to the side chain of Asp228 through one of the carboxyl O atoms (see Fig. 2*b*). The bound Bicine molecule coordinates the Cd3 metal ion and displaces the conserved water molecule (wat2) observed in both the *T. maritima* and *E. coli* endonuclease IV structures along with a second water molecule (wat3) that is only observed in the *E. coli* endonuclease IV structure. No other significant structural differences in the active-site region were observed between *T. maritima* endonuclease IV bound to cadmium and zinc and *E. coli* endonuclease IV bound to zinc.

4. Discussion

The X-ray crystal structures of the *T. maritima* endonuclease IV homologue reveal divalent metal ions bound in the active-site region. Consequently, observation of the structural interplay between the protein and selective metal coordination further characterizes the AP endonuclease family of enzymes. One structure of *T. maritima* endonuclease IV contains three zinc ions bound in the active-site region. The second structure is likely to contain a mixed-metal configuration of two cadmium ions and one zinc ion bound in the active-site region. These structures of *T. maritima* endonuclease IV further revealed the use of the eight-stranded $\alpha\beta$-barrel fold (TIM barrel; Banner *et al.*, 1975) for DNA binding and catalysis in the AP endonuclease superfamily. Furthermore, the presence of a trinuclear metal binding site in the active site of the respective *T. maritima* endonuclease IV structures further establishes the binding of trinuclear metal ions as a necessary motif for the AP endonuclease family of enzymes. Based on the previously characterized AP endonuclease activity (Haas *et al.*, 1999) and the overall structural similarity of the *T. maritima* endonuclease IV and *E. coli* endonuclease IV enzymes, it is likely that *T. maritima* endonuclease IV binds AP-DNA substrate in a similar manner to that previously described for *E. coli* endonuclease IV (Hosfield *et al.*, 1999; Garcin *et al.*, 2008). DNA binding to *T. maritima* endonuclease IV is likely to be mediated by interactions between the R-loop regions that emanate from the C-terminal end of the TIM-barrel fold and the negatively charged DNA phosphate backbone. The conserved TIM-barrel fold of *T. maritima* endonuclease IV positions the five R-loop regions to form an interface that resembles the known AP-DNA-binding interface for *E. coli* endonuclease IV (Hosfield *et al.*, 1999; Garcin *et al.*, 2008). In *T. maritima* endonuclease IV the conserved residues Arg37 (R-loop 2) and Tyr72 (R-loop 3) may interact with AP-DNA substrate in a similar manner to that described for *E. coli* endonuclease IV, where R-loop conformational changes provide specific interactions with DNA to promote DNA bending. These residues have been shown to interact specifically with the minor groove of the AP-DNA substrate, in which residue Tyr72 base-stacks with the base pair 5′ to the AP site to occupy the gap left by the extrahelical AP site and residue Arg37 forms a base-stacking interaction with the base pair 3′ to the AP site (Hosfield *et al.*, 1999; Garcin *et al.*, 2008). Thus, the key structural features that have been shown to be responsible for AP-RNA recognition and binding of the scissile phosphate to the trinuclear metal site in the active-site region in *E. coli* endonuclease IV (Hosfield *et al.*, 1999; Garcin *et al.*, 2008) are also present in *T. maritima* endonuclease IV. In the absence of an AP-DNA substrate bound to *T. maritima* endonuclease IV, further structural studies of complexes with substrate will be needed to fully characterize the specific DNA-binding interactions related to the recognition of AP-DNA.

Previous mutational (Ishchenko *et al.*, 2006; Yang *et al.*, 1999), structural (Hosfield *et al.*, 1999; Garcin *et al.*, 2008) and molecular-dynamics simulation (Ivanov *et al.*, 2007) studies on the *E. coli* endonuclease IV enzyme have shown that all three zinc ions participate directly in a three-metal-ion mechanism in which an adjacent hydroxide bridging Zn1 and Zn2 is positioned to be the attacking nucleophile for cleavage of the scissile phosphate bond of AP-DNA. It has been proposed that residue Glu261 in *E. coli* endonuclease IV (conserved residue Glu260 in *T. maritima* endonuclease IV) participates in activating the hydroxide nucleophile (Garcin *et al.*, 2008; Ivanov *et al.*, 2007). Even with such a low sequence identity the residues that are involved in forming the trinuclear metal binding site are absolutely conserved in both the *T. maritima* endonuclease IV and *E. coli* endonuclease IV structures (see Figs. 2*a*, 2*b* and 5).

A structural analysis of the three active-site regions of *T. maritima* endonuclease IV bound to either trinuclear zinc or the possible mixed-metal configuration of two cadmium ions and one zinc ion and *E. coli* endonuclease IV bound to trinuclear zinc revealed that the active-site structure and coordination to metal sites 1 and 2 is conserved in all three structures (see Figs. 2*a*, 2*b* and 5). However, occupancy refinements of the respective metal ions in the *T. maritima* endonuclease IV structures show that metal site 1 may not be fully occupied when divalent cadmium is present in the active site in both metal sites 2 and 3. In the structure bound to cadmium and zinc the refined occupancy value for metal site 1 (Zn1, 44%) suggests that a zinc ion (or possibly a cadmium ion) does not completely occupy this site, whereas in the structure of *T. maritima* endonuclease IV bound to trinuclear zinc the Zn1 metal ion refined to a higher occupancy value (Zn1, 82%), suggesting that metal site 1 is nearly fully occupied by zinc. It has been shown that cadmium can compete with divalent zinc binding to proteins. Specifically, cadmium has a preference for cysteine, glutamate, aspartate and histidine ligands in tetrahedral geometries (McMurray & Tainer, 2003). It has been suggested that heavy-metal-ion toxicity may disrupt the metal-site geometry as cadmium ions can replace zinc ions to become an environmental mutagen (Garcin *et al.*, 2008; McMurray & Tainer, 2003). In the *T. maritima* endonuclease IV active site, metal site 1 coordinates to the side chains of His69, His109 and Glu144 and water molecule 1 (wat1) in a tetrahedral arrangement and is in an ideal geometry for either zinc or cadmium binding. The presence of a partially bound zinc or cadmium ion in metal site 1 does not disrupt the coordination geometry of the partially occupied metal site 1 in comparison to either the structure of *T. maritima* endonuclease IV or *E. coli* endonuclease IV with zinc bound in site 1. Further studies involving the effects of heavy-metal-ion binding to *T. maritima* endonuclease IV are necessary to understand the impact of metal binding with respect to catalytic activity. The observation that metal site 1 is also partially inaccessible to solvent cannot be ruled out as a possible

explanation for the low-occupancy binding of zinc to metal site 1 in the mixed-metal configuration of *T. maritima* endonuclease IV.

As initially shown in the structure of wild-type *E. coli* endonuclease IV (Hosfield *et al.*, 1999), the third metal site (Zn3) is mostly solvent-accessible and is coordinated in a distorted trigonal bipyramidal arrangement (see Fig. 5). Additional structures of phosphate-bound (E261Q mutant; distorted trigonal bipyramidal Zn3 geometry) and both AP-DNA substrate (E261Q mutant; trigonal Zn3 geometry) and product complexes (both wild-type and Y72A mutant; trigonal bipyramidal Zn3 geometry) of *E. coli* endonuclease IV have suggested that the coordination geometry around metal site 3 varies extensively throughout catalysis (Hosfield *et al.*, 1999; Garcin *et al.*, 2008). In the structures of *T. maritima* endonuclease IV, metal site 3 is coordinated in a distorted tetrahedral arrangement when bound to zinc, whereas metal site 3 is coordinated in a distorted trigonal bipyramidal arrangement when bound to cadmium and Bicine (see Figs. 2*a* and 2*b*). The coordination around metal site 3 in the zinc-bound structure closely resembles the structure of the *E. coli* endonuclease IV E261Q mutant bound to phosphate. The phosphate O atom coordinating Zn3 in the *E. coli* endonuclease IV structure is located in nearly the same position as water molecule 2 in *T. maritima* endonuclease IV. Additionally, the coordination around metal site 3 in the mixed-metal configuration of the *T. maritima* endonuclease IV structure bound to cadmium and Bicine resembles the structure of the *E. coli* endonuclease IV E261Q mutant–DNA substrate complex. In both structures the Zn3 coordination sphere is incomplete as the coordinating side-chain residues are arranged in a trigonal geometry in which only one of the carboxyl atoms in the side chains of Asp229 in the *E. coli* structure and Asp228 in the *T. maritima* structure coordinate to Zn3. In the structure of the *E. coli* endonuclease IV E261Q mutant–DNA substrate complex both the 3′-O atom of the intact phosphodiester bond and the unesterified phosphate O atom are constrained, which prevents completion of the Zn3 coordination sphere. In the *T. maritima* endonuclease IV structure bound to cadmium and Bicine, the Zn3 coordination sphere is completed by a bidentate interaction with Bicine through O4 and O22. Further structural studies of *T. maritima* endonuclease IV will be needed in order to assess the significance of these structural observations in relation to catalysis. However, these results provide further evidence that the coordination geometry around metal site 3 is quite variable and are in agreement with previous structural results on *E. coli* endonuclease IV that suggest that the Zn3 coordination sphere is variable throughout the catalytic mechanism in order for these enzymes to possess such remarkable substrate recognition and specificity toward AP-site DNA. Thus, these structural studies of the *T. maritima* endonuclease IV homologue further reveal the use of the TIM-barrel fold and the trinuclear metal binding site as key structural elements involved in AP-site repair processes that are highly conserved from bacteria to humans and archaea. Future activity and structural studies of *T. maritima* endonuclease IV in complex with both AP-DNA and catalytic divalent metal ions, including toxic heavy-metal ions such as cadmium, will be important for further characterization of the role of the AP endonuclease family of enzymes in the BER pathway.

We thank Dr Jenny P. Glusker for a critical review of the manuscript and valuable comments. This research was sponsored by the Laboratory Directed Research and Development Program of Oak Ridge National Laboratory (ORNL), managed by UT-Battelle LLC for the US Department of Energy under Contract No. DE-AC05-00OR22725. The research at Oak Ridge National Laboratory's Center for Structural Molecular Biology (CSMB) was supported by the Office of Biological and Environmental Research, using facilities supported by the US Department of Energy, managed by UT-Battelle LLC under contract No. DE-AC05-00OR22725.

References

Adams, P. D., Grosse-Kunstleve, R. W., Hung, L.-W., Ioerger, T. R., McCoy, A. J., Moriarty, N. W., Read, R. J., Sacchettini, J. C., Sauter, N. K. & Terwilliger, T. C. (2002). *Acta Cryst.* D**58**, 1948–1954.
Afonine, P. V., Grosse-Kunstleve, R. W. & Adams, P. D. (2005). *CCP4 Newsl.* **42**, contribution 8.
Aravind, L., Walker, D. R. & Koonin, E. V. (1999). *Nucleic Acids Res.* **27**, 1223–1242.
Bailly, V. & Verly, W. G. (1989). *Nucleic Acids Res.* **17**, 3617–3618.
Banner, D. W., Bloomer, A. C., Petsko, G. A., Phillips, D. C., Pogson, C. I., Wilson, I. A., Coran, P. H., Furth, A. J., Milman, J. D. & Offord, R. E. (1975). *Nature (London)*, **255**, 609–614.
Barzilay, G. & Hickson, I. D. (1995). *Bioessays*, **17**, 713–719.
Chen, V. B., Arendall, W. B., Headd, J. J., Keedy, D. A., Immormino, R. M., Kapral, G. J., Murray, L. W., Richardson, J. S. & Richardson, D. C. (2010). *Acta Cryst.* D**66**, 12–21.
Collaborative Computational Project, Number 4 (1994). *Acta Cryst.* D**50**, 760–763.
Corfu, N. A. & Bin Song, L. J. (1992). *Inorg. Chim. Acta*, **192**, 243–251.
Cunningham, R. P. (1997). *Mutat. Res.* **383**, 189–196.
DeLano, W. L. (2008). *PyMOL Molecular Viewer*. DeLano Scientific LLC, Palo Alto, California, USA. http://www.pymol.org.
Demple, B., Herman, T. & Chen, D. S. (1991). *Proc. Natl Acad. Sci. USA*, **88**, 11450–11454.
Demple, B., Johnson, A. & Fung, D. (1986). *Proc. Natl Acad. Sci. USA*, **83**, 7731–7735.
Doetsch, P. W. & Cunningham, R. P. (1990). *Mutat. Res.* **236**, 173–201.
Emsley, P. & Cowtan, K. (2004). *Acta Cryst.* D**60**, 2126–2132.
Farber, G. K. & Petsko, G. A. (1990). *Trends Biochem. Sci.* **15**, 228–234.
Garcin, E. D., Hosfield, D. J., Desai, S. A., Haas, B. J., Björas, M., Cunningham, R. P. & Tainer, J. A. (2008). *Nature Struct. Mol. Biol.* **15**, 515–522.
Haas, B. J., Sandigursky, M., Tainer, J. A., Franklin, W. A. & Cunningham, R. P. (1999). *J. Bacteriol.* **181**, 2834–2839.
Hitomi, K., Iwai, S. & Tainer, J. A. (2007). *DNA Repair*, **6**, 410–428.
Hosfield, D. J., Guan, Y., Haas, B. J., Cunningham, R. P. & Tainer, J. A. (1999). *Cell*, **98**, 397–408.
Hughes, R. C., Tomanicek, S. J., Ng, J. D. & Coates, L. (2009). *Acta Cryst.* F**65**, 1317–1319.
Huffman, J. L., Sundheim, O. & Tainer, J. A. (2005). *Mutat. Res.* **577**, 55–76.
Hutchinson, F. (1985). *Prog. Nucleic Acid Res. Mol. Biol.* **32**, 115–154.
Ishchenko, A. A., Deprez, E., Maksimenko, A., Brochon, J.-C., Tauc, P. & Saparbaev, M. K. (2006). *Proc. Natl Acad. Sci. USA*, **103**, 2564–2569.
Ishchenko, A. A., Sanz, G., Priveventzev, C. V., Maksimenko, A. V. & Saparbaev, M. (2003). *Nucleic Acids Res.* **31**, 6344–6353.
Ischenko, A. A. & Saparbaev, M. K. (2002). *Nature (London)*, **415**, 183–187.
Ishchenko, A. A., Yang, X., Ramotar, D. & Saparbaev, M. (2005). *Mol. Cell. Biol.* **25**, 6380–6390.
Ivanov, I., Tainer, J. A. & McCammon, J. A. (2007). *Proc. Natl Acad. Sci. USA*, **104**, 1465–1470.
Kerins, S. M., Collins, R. & McCarthy, T. V. (2003). *J. Biol. Chem.* **278**, 3048–3054.
Krissinel, E. & Henrick, K. (2004). *Acta Cryst.* D**60**, 2256–2268.
Krokan, H. E., Standal, R. & Slupphaug, R. (1997). *Biochem. J.* **325**, 1–16.
Leslie, A. G. W. (1992). *Jnt CCP4/ESF–EACBM Newsl. Protein Crystallogr.* **26**.
Levin, J. D. & Demple, B. (1990). *Nucleic Acids Res.* **18**, 5069–5075.
Levin, J. D., Johnson, A. W. & Demple, B. (1988). *J. Biol. Chem.* **263**, 8066–8071.
Lindahl, T., Karran, P. & Wood, R. D. (1997). *Curr. Opin. Genet. Dev.* **7**, 158–169.
Loeb, L. A. & Preston, B. D. (1986). *Annu. Rev. Genet.* **20**, 201–230.
Marsic, D., Hughes, R. C., Byrne-Steele, M. L. & Ng, J. D. (2008). *BMC Biotechnol.* **8**, 44.
McCoy, A. J., Grosse-Kunstleve, R. W., Adams, P. D., Winn, M. D., Storoni, L. C. & Read, R. J. (2007). *J. Appl. Cryst.* **40**, 658–674.
McMurray, C. T. & Tainer, J. A. (2003). *Nature Genet.* **34**, 239–241.
Mol, C. D., Hosfield, D. J. & Tainer, J. A. (2000). *Mutat. Res.* **460**, 211–229.
Otwinowski, Z. & Minor, W. (1997). *Methods Enzymol.* **276**, 307–326.
Ramotar, D. (1997). *Biochem. Cell Biol.* **75**, 327–336.

Reardon, D. & Farber, G. K. (1995). *FASEB J.* **9**, 497–503.
Sobol, R. W., Kartalou, M., Almeida, K. H., Joyce, D. F., Engelward, B. P., Horton, J. K., Prasad, R., Samson, L. D. & Wilson, S. H. (2003). *J. Biol. Chem.* **278**, 39951–39959.
Thompson, J. D., Higgins, D. G. & Gibson, T. J. (1994). *Nucleic Acids Res.* **22**, 4673–4680.
Yang, X., Tellier, P., Masson, J. Y., Vu, T. & Ramotar, D. (1999). *Biochemistry*, **38**, 3615–3623.